Journal of Power Sources 225 (2013) 101–107

Contents lists available at SciVerse ScienceDirect

Journal of Power Sources

journal homepage: www.elsevier.com/locate/jpowsour

A high-capacity carbon prepared from renewable chicken feather biopolymer for supercapacitors

Qiang Wang, Qi Cao*, Xianyou Wang, Bo Jing, Hao Kuang, Ling Zhou

Key Laboratory of Environmentally Friendly Chemistry and Applications of Minister of Education, College of Chemistry, Xiangtan University, Xiangtan 411105, China

HIGHLIGHTS

- Chicken feather carbon is acted as electrode materials for the first time.
- Chicken feather originates from essentially free renewable livestock biowaste.
- There are abundant micropores for the activated chicken feather carbon.
- The activated carbon shows the excellent electrochemical properties.

ARTICLE INFO

Article history:
Received 13 July 2012
Received in revised form
25 September 2012
Accepted 10 October 2012
Available online 17 October 2012

Keywords:
Supercapacitor
Activated carbon
Chicken feather
Electrode material

ABSTRACT

Micropopous chicken feather carbon (CFC) severing as electrode materials for the first time is prepared via the activation with KOH agent to different extents. The structure and electrochemical properties of CFC materials are characterized with N_2 adsorption/desorption measurements, X-ray diffraction (XRD), transmission electron microscope (TEM), cyclic voltammetry (CV), galvanostatic charge/discharge cycling and electrochemical impedance spectroscopy (EIS). The obtained results show that CFC activated by KOH with KOH/CFC weight ratio of 4/1 (CFCA4) possesses the specific surface area of 1839 $m^2\ g^{-1}$, average micropore diameter of 1.863 nm, and exhibits the highest initial specific capacitance of 302 $F\ g^{-1}$ at current density of 1 $A\ g^{-1}$ in 1 M H_2SO_4, and that even after 5000 cycles, CFCA4 specific capacitance is still as high as 253 $F\ g^{-1}$. Furthermore, CFCA4 also delivers specific capacitance of 181 $F\ g^{-1}$ at current density of 5 $A\ g^{-1}$ and 168 $F\ g^{-1}$ at current density of 10 $A\ g^{-1}$. Accordingly, the microporous activated carbon material derived from chicken feather provides favorable prospect in electrode materials application in supercapacitors.

1. Introduction

As a novel environmentally friendly power storage device, supercapacitors have received intense interests in recent years, which bridge the gap between the high-capacity rechargeable batteries and traditional capacitors with pulsed high power output [1,2]. Supercapacitors can not only provide high specific power (10 $kW\ kg^{-1}$), a long cycle lifetime ($>10^5$) and rapid charge/discharge processes, but also retain higher energy density than conventional capacitors [3–5]. Hence, supercapacitors stimulate extensive application serving as the primary source or the assistant source. Currently, with the exponential growth in the market of portable electronic devices and hybrid electric vehicles, supercapacitors with light-weight and compact electric power sources are desired. Therefore, to meet the tremendous needs in practical application, many strategies are under development for optimizing the high energy density of capacitor while retaining a high specific power.

Thus, various electrode materials for supercapacitors have been investigated, including metal oxides, conducting polymers and diverse types of carbon materials. Although hydrous RuO_2 ($RuO_2{\cdot}xH_2O$) [6] and MnO_2 [7] have been tested to possess a capacitance as high as 1300 $F\ g^{-1}$, the high cost of precious metals such as ruthenium (Ru), the low surface and poor electrical conductivity of alternative metals, such as manganese (Mn), limits their practical application. Furthermore, electronically conducting polymers (such as polyaniline, polypyrrole, plyphene) also present poor stability associated with swelling and attenuation during cycling.

Recently, numerous carbonaceous materials, such as nanotubes, fibers and tubes, have been utilized as the electrode materials of electrical double-layer capacitors (EDLCs). In various carbon-based

* Corresponding author. Tel./fax: +86 731 58298090.
E-mail address: wjcaoqi@163.com (Q. Cao).

0378-7753/$ – see front matter © 2012 Elsevier B.V. All rights reserved.
http://dx.doi.org/10.1016/j.jpowsour.2012.10.022

electrode materials for EDLCs, activated carbons have been in the spotlight [8–11] because of its abundant raw materials, relatively low manufacturing cost, high specific surface area, good electrical conductivity and broad working media (range from strongly acidic to strongly basic ones). Generally, as EDLCs utilizing the electric double layer to store energy when charges accumulate electrostatically at the electrode/electrolyte interface [9,12], it is believed that the activated carbons with large specific surface area and suitable pore size distribution would provide higher capacitance and more energy. However, the performance of EDLCs is correlated with the pore distribution and the types of porosity, and also extensively depends on the types of the employed precursor materials and different activation methods [13,14].

While activated carbons have been produced by different activation methods (physical activation, chemical etching) from various precursors, only a few researchers focus on biomass or their derivatives. One example is the carbonization of a chicken eggshell membrane biopolymer for supercapacitor electrode material [15]. Taking the potential scale of supercapacitor application into account, the employment of renewable biomaterials to prepare carbon materials would be regard as more worthwhile. In this respect, microporous carbon material derived from chicken feather has been prepared for electrode material. On one hand, chicken feather is composed of α-helix keratin tubes that are filled with β-helix keratin [16]. After carbonization and activation, the hollow nature of chicken feather and its a-helix structure can allow a uniform structured microporous material with high surface area. On the other hand, chicken feather originates from abundant and essentially free renewable biomasses. With the growing of poultry industry, approximate 4 billion pounds of chicken feather is produced per year in USA [17]. Therefore, converting chicken feather into electrode materials may be supposed to an economical and environmentally friendly route. In the paper, the physical properties such as Brunauer–Emmett–Teller (BET) surface-area, pore-size distribution, total pore volume and microstructure, were analyzed as a function of the KOH/CFC ratio in detail. The electrochemical characteristics of the prepared samples for electrode materials were also investigated in H_2SO_4 electrolyte.

2. Experimental section

2.1. Preparation of activated chicken feather carbons

Chicken feather used in the experiments was collected from poultry market. Firstly, chicken feather was washed with distilled water and dried at 60 °C for 24 h under air atmosphere. Subsequently, the chicken feather was heated (the heating rate is 2 °C min^{-1}) at 210 °C for 26 h in argon (Ar) atmosphere. In the process, the chicken feather crosslinked naturally. Thereafter, the temperature was raised (the rate heating is 5 °C min^{-1}) from 210 °C to the final temperature of 450 °C, then the temperature at 450 °C was held for 1 h in the presence of Ar [16]. Secondly, the CFC powder was impregnated in KOH solution containing 4 ml of water and ethanol (the weight ratio of water: ethanol = 4:1) at room temperature. The weight ratio of KOH/CFC ranged between 1 and 5. After sufficient mixing, the KOH/CFC slurry was pretreated at 120 °C for 48 h in air. Thirdly, the dried samples were grinded and heat-treated in tubular resistance furnace, and then activated at a heating ratio of 5 °C min^{-1} from room temperature to 800 °C. Then the samples maintained the temperature at 800 °C for 1 h in Ar atmosphere. Finally, the etched products were washed first with 1 M HCl solution, ethanol and distilled water in sequence at ambient temperature. Leaching was carried out for several times until the pH value of the water-carbon mixture was about 7. The leached products were then dried in vacuum at 60 °C for 24 h. According to the mixing weight ratios (KOH/CFC), the samples were designated as CFCA0 (0/1), CFCA1 (1/1), CFCA2 (2/1), CFCA3 (3/1), CFCA4 (4/1) and CFCA5 (5/1).

2.2. Chicken feather carbon characterization

High-resolution transmission electron microscope (HR-TEM) measurements were conducted on JEOL 2010F microscope operated at 5 keV beam energy, to reveal the micro-morphology of CFC samples. Nitrogen adsorption/desorption isotherm were measured on a (Quantachrome Corp. Nova-2000e gas sorption analyzer) sorptiometer at 77 K (−196 °C). All carbon samples should be previously outgassed in vacuum at 398 K for 24 h. From the nitrogen adsorption isotherms, the specific surface area and micropore volume of the activated samples was evaluated with the application of the BET and t-plot method, respectively. The pore size distribution of these samples was determined by the Barrett–Joyner–Halenda (BJH) method. The total amounts of N_2 adsorbed, which corresponds approximately to the sum of the micropore and mesopore volumes, were calculated at a relative pressure of $P/P_0 = 0.99$. The crystallographic structures of the prepared materials were detected by a power X-ray diffraction (XRD) system (*D*/max 2500) equipped with CuKα radiation (λ = 0.15418 nm), and X-ray photoelectron spectroscopy (XPS) results were recorded with a K-Alpha 1063 spectrometer using an AlKα monochromatic source (12 kV, 6 mA).

2.3. Electrochemical measurements

The supercapacitor electrodes were made of different activated chicken feather carbons (CFCAs), acetylene black and polyvinylidenefluoride (PVDF). Prior to the formation of electrodes for electrochemical performance test, Acetylene black and PVDF were added into *N*-methyl pyrrolidinone (NMP) solution, and then CFCAs were added to the mixed solution severally. CFCAs, acetylene black and PVDF were mixed according to the weight ratio of 80:10:10 at ambient temperature. After sufficient stirring, the mixture was pressed onto a steel mesh with a size of 1 cm^2 (the steel mesh functions as the current collector), yielding electrodes with the thickness of 0.2 mm and the active mass of 3–5 mg. Before the electrochemical test, the prepared electrodes were dried at 60 °C for 24 h in vacuum. Sandwich-type capacitors, composed of a pair of electrodes and a piece of filter paper as the separator, were used to examine the electrochemical performance of CFCAs. All electrochemical measurements were performed at ambient temperature in 1 M H_2SO_4 electrolytes. Potentiodynamic CV (1, 10, 50, 100 mV s^{-1}) and electrochemical impedance spectroscopy (EIS) (10^{-3}–10^5 Hz, amplitude of signal 5 mV) measurement were conducted in an electrochemical workstation (Zahner Im6ex). The capacitance behaviors of CFCAs electrodes were evaluated through galvanostatic charge/discharge cycling in the potential range between 0 and 1.0 V at different current density (1, 5, 10 A g^{-1}) with Neware battery test system (BTS-XWJ-6.9.27s) multichannel generator, as well as through multi-cycle charge/discharge at a current density of 1 A g^{-1}.

3. Results and discussion

3.1. Pore structural properties

Those typical N_2 adsorption/desorption isotherms of all CFCAs prepared according to different KOH/CFC activation ratios, as shown in Fig. 1, reveal the low-pressure extent where adsorption occurs. The linear plot of N_2 isotherms reveals pore characteristic and type of hysteresis loops. As illustrated in the figure, major adsorption of CFCA1 and CFCA2 occurs at low relative pressure of

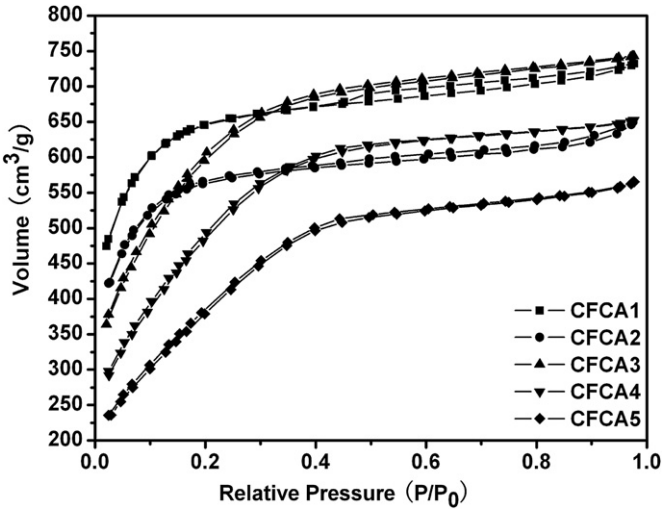

Fig. 1. Nitrogen adsorption/desorption isotherms analysis at 77 K on activated chicken feather carbons prepared as a function of the weight ratio of KOH/CFC.

less than 0.15, giving rise to an almost horizontal plateau at higher relative pressures. These curves indicate that CFCA1 and CFCA2 possess the high microporosity and narrow pore size distribution. Additionally, the hysteresis loops can be observed distinctly at the relative pressure between 0.5 and 0.99, indicating the existence of a certain amount of mesopore. For the rest three activated samples, the relative pressure at horizontal plateau stage during nitrogen uptake gradually rises with the increase in the KOH/CFC weight ratio, suggesting that the additional neo-pore has developed and certain quantity of micropore has been enlarged. Therefore, the adsorption isotherms illustrate the relatively inhomogeneous pore diameter of CFCA3, CFCA4, and CFCA5. From the N_2 adsorption/desorption plot, these adsorption/desorption isotherms are consistent with type I and H4 hysteresis loops (according to the IUPAC classification) [18,19], which is indicative of microporous materials with slit shape pore system. The different pore size distribution and microporous type could be caused by different weight ratios of KOH versus CFC.

Fig. 2 displays the Barret, Joyner, and Halenda (BJH) pore-size distributions curves of all the activated samples. It is clearly observed that the maximum peak shifts from ~1.25 to ~2.00 nm with the activated weight ratio varying from 1 to 5. Exceptionally, CFCA4 exhibits the maximum peak at ~2.00 nm. Comparatively,

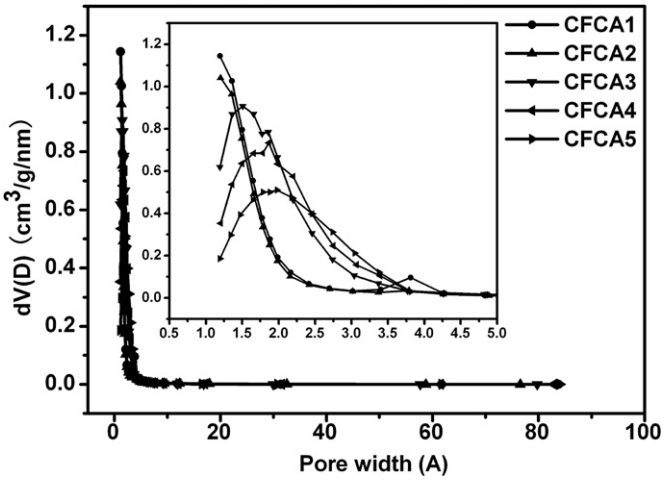

Fig. 2. The pore size distribution of activated CFC.

the CFCA1 and CFCA2 possess a relatively centralized pore size distribution, and the pore size of the rest three samples has broad pore distribution. The most extensive pore size ranges from ~1.20 to ~3.75 nm for CFCA4. The variation manner of pore size distribution is well consistent with the concept of pore-width development, which results from the repetition of collapse and recombination of pores by KOH activation. Generally, the chemical reactions of hydroxide/carbon often promote the development of micropores and enlarge the developed microspores [20,21]. Additionally, Table 1 summarizes the pore structural properties of CFCAs calculated according to the BET equation and the t-plot method from the nitrogen adsorption isotherms at 77 K. Before the activation, CFCA0 only exhibits a specific surface area of 0.568 $m^2\ g^{-1}$. However, after the treatment with KOH etching, the specific surface area is amplified to 1454–2385 $m^2\ g^{-1}$, and the average pore diameter is increased gradually from 1.196 to 1.977 nm as well. Certainly, microporous surface area is reduced significantly with the increasing of etching ratio at high temperature. The interior etching process of KOH activation is responsible for the specific surface and pore size modification [22].

3.2. Microstructure characterization of CFCA0 and CFCA4

The HR-TEM images in Fig. 3 show the microstructure of CFCA0 and CFCA4. As seen from Fig. 3a and c, the activation with KOH does not destroy the intrinsic non-crystalline with parallelism of graphene multi-layered structure of the material. Furthermore, from image-analysis results of Fig. 3a and c, abundant neo-micropore has been developed by the means of the chemical activation. It is suggested that the activation reaction between alkali hydroxide and CFC proceed as $6KOH + 2C \leftrightarrow 2K_2CO_3 + 3H_2 + 2K$, followed by decomposition of K_2CO_3 and/or reaction of $K/K_2CO_3/CO_2$ simultaneously [23]. Additionally, Fig. 3b and d reveals a randomly distributed porous morphology in CFCA0 and CFCA4. It is obvious that the activation yields extremely small size, ranging from ~1 to ~2 nm. These images substantially indicate that the activation process etches the CFC and has significantly enlarged porous structure, which is in accordance with the adsorption of N_2 pore distribution results.

Characterization of samples CFCA0 and CFCA4 by means of XRD and XPS are shown in Fig. 4a and b. As illustrated from the XRD patterns, the crystallites in two samples have a scattering angle (2θ) near 26°. Compared with CFCA0, CFCA4 has the obviously reduced intensity and the (002) distinctly broadened peak. It further corroborates that the crystalline structures have been markedly destroyed in the chemical etching process. It is deduced that CFCA4 is consistent with the presence of a high density of pores. According to the XPS C1s spectrum results shown in Fig. 4b, any shift in the C1s peak is marked in activated carbon, further attesting the impossible charge transfer reaction in the process of activation with KOH. The phenomenon signifies the identical structure of all samples. Moreover, the salient points between 286 and 290 eV is owing to C–O groups and energy loss "shake-up" features [24]. A large number of oxygen-containing groups are mightily suppressed after activation, with two small new peaks emerging between 292 and 296 eV in the CFCA4. The new salient points are designed as K2p peaks. The potassium residue primarily derived from K_2CO_3 with trace amount of KOH is responsible for the development of K2p peaks (<1.4 atomic % as detected from XPS).

3.3. Electrochemical features

On the basis of different activated carbon materials, the CV test was conducted in 1 M H_2SO_4 from −0.5 to 0.5 V at the scanning rates of 1, 10, 50 and 100 mV s^{-1} Fig. 5 presents the CV curves of

Table 1
Porosity parameters of chemical activated chicken feather carbons calculated from nitrogen desorption isotherms and ESR data calculated from the *X*-intercept of the Nyquist plot.

Samples	BET surface area ($m^2\ g^{-1}$)	Micropore surface area ($m^2\ g^{-1}$)	Total pore volume ($cm^3\ g^{-1}$)	Micropore volume ($cm^3\ g^{-1}$)	Average pore diameter (nm)	ESR (Ω)
CFCA0	0.568	–	0.001	–	–	0.86
CFCA1	2426	2096	0.870	0.856	1.196	0.67
CFCA2	2126	1838	0.788	0.747	1.203	2.28
CFCA3	1911	1192	1.169	0.508	1.506	0.97
CFCA4	1839	1575	1.069	0.850	1.863	0.43
CFCA5	1398	1020	0.922	0.555	1.977	0.37

ESR: equivalent series resistance.

CFCA0 and CFCA4. With the increasing of scan rates, rectangular curves of CFCA0 show a distinctly distortion (Fig. 5a), reflecting a more significant ohmic resistance in pores. The more serious distortion of CV plot of CFCA0 at high scanning rates can be attributed to its plentiful micropores (<1 nm) which are somewhat close to or smaller than the adsorption ion size. Here, the capacity of this sample is calculated from equation:

$$C = 2(|I_a| + |I_c|)/M(dv/dt) \quad (1)$$

where C is the specific capacitance of a single electrode in the capacitor, I_a and I_c represents the anodic and cathodic charging current, respectively; M is the total activated mass of two electrodes; dv/dt is the scan rate. The specific capacitance at the mid-range potential is only 12 F g^{-1}, implying that the majority of pore can not be well penetrated at the scanning rate of 1 mV s^{-1} [25]. The results may be also related to the low specific surface area (0.568 $m^2\ g^{-1}$). Generally, as theoretically supplied, the specific capacitance is proportional to the surface area for adsorption of electrolytes of activated carbons [25]. However, compared with the untreated carbon material, CFCA4 (BET specific surface area: 1839 $m^2\ g^{-1}$; average pore diameter: 1.863 nm) shows the quite rectangular shape of CV curves at various scanning rates (Fig. 5b), suggesting the typical of capacitive and reversible behavior after the activation, and the high enough conductivity to assure excellent charge propagation. These behaviors are in consistence with the EIS testing results. Theoretically, the quasi-rectangular CV curves, in which the current rapidly reaches a truly horizontal level after the reversal of the voltage sweep, can be emerged if the interface forming the double layer is homogeneous and ideally polarizable [13]. In fact, as the sweep rate increases from 1 to 100 mV s^{-1}, the delay phenomenon of the current to reach a horizontal value after reversal of the potential sweep is aggravated. The enhancement of the ohmic resistance in the electrolyte along the axial direction of micropores and the distributed capacitance effect in porous electrodes is responsible for postponement of the current inversion upon increasing the voltage sweep rate [26]. Besides, for CFCA4 two-electrode capacitor, the quite small humps in CV curves are

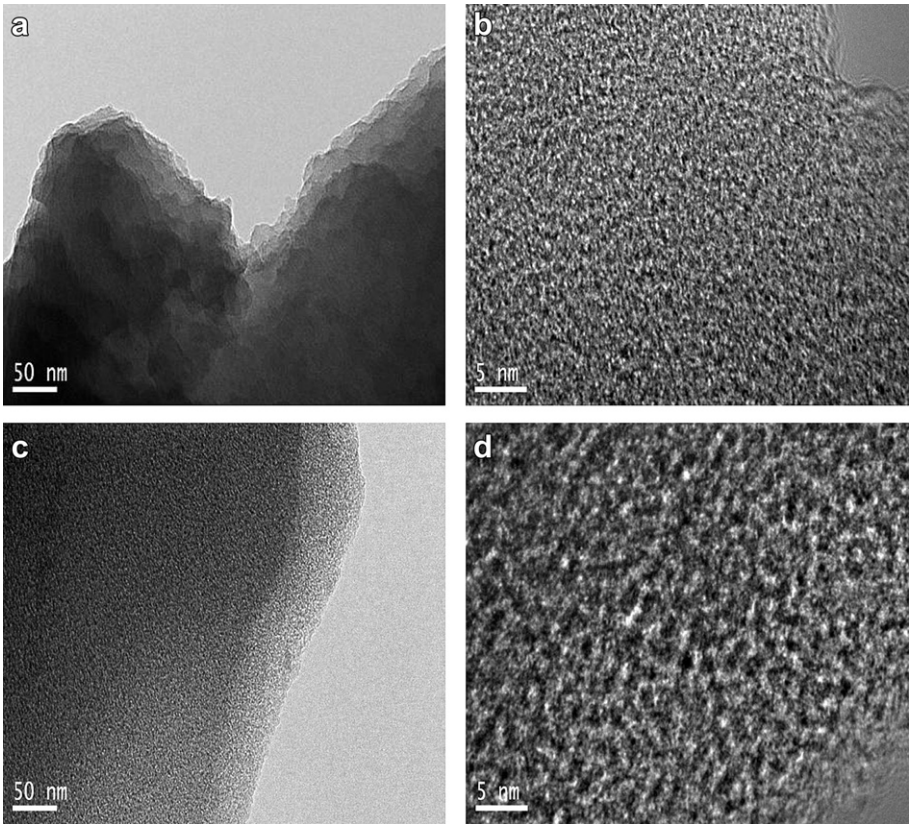

Fig. 3. a), c) Low and b), d) high magnification high-resolution TEM images of CFCA0 and CFCA4.

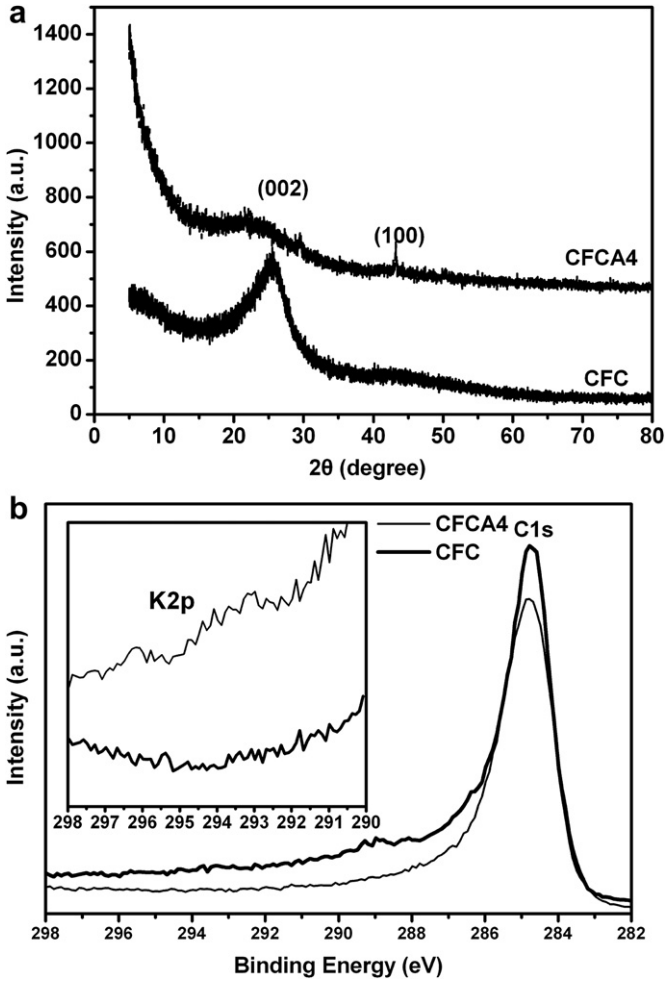

Fig. 4. Characterization of CFCA0 and CFCA4 material a) power XRD pattern (plotted as Cu Kα), b) XPS C1s spectra, with K2p region in the inset.

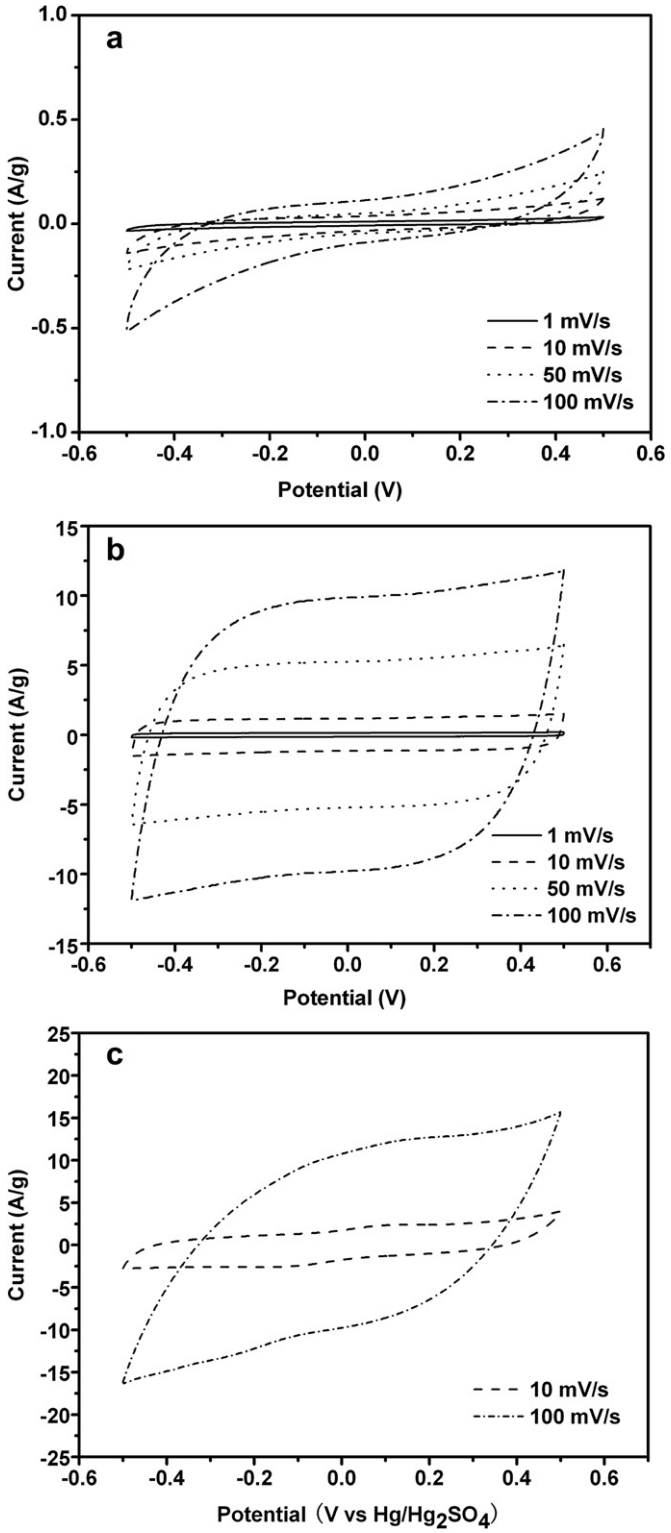

Fig. 5. Electrochemical cyclic voltammograms performance of a) CFCA0 and b) CFCA4 carbons using a two-electrode cell, c) CFCA4 carbons using a three-electrode cell in 1 M H_2SO_4. The current density is calculated based on the weight of a single electrode. Reference electrode: Hg/Hg_2SO_4.

observed at around 0.2 and −0.2 V, indicating that some redox processes contribute to the electrochemical properties of the material. In order to state the contribution of redox reactions well, CV curves, as shown in Fig. 5c, were measured versus the Hg/Hg_2SO_4 reference electrode in a three-electrode cell using the CFCA4 material as the working electrode and platinum electrode as the counter electrode. Unsurprisingly, the CV curves exhibit a pair of small and broad humps at scanning rates of 10 and 100 mV s^{-1}. Considering that the minority of oxygen-containing groups was detected by XPS in CFCA4, we deduced that these humps derive from the redox reaction of oxygen surface functionality. Generally, for activated carbons, these redox peaks are traditionally assigned to electrochemical reactions of oxygen surface functionalities such as quinine–hydroquinone pair [27].

The impedance spectra analysis of the frequency ranging from 10^5 to 10^{-3} Hz yields the Nyquist plot in Fig. 6. The plot features two distinct traits: a high-frequency semicircle and a low frequency spike. In the range of high-frequency, the intercept of the semicircle with the real axis represents equivalent series resistance (ESR), including the resistance of the electrolyte solution, the intrinsic resistance of activation material, and the contact resistance of the interface active material/current collector [28,29]. The ESR values of all samples were estimated from the *X*-intercept of the Nyquist plot, which is also shown in Table 1. It's clear that the lower ESR values of CFCA4 and CFCA5 are respectively about 0.43 and 0.37 Ω. Moreover, the semicircle loop validates the faradic charge-transfer resistance that dominated by the process of ion transport in the porous electrode. As far as we know, the smaller radius of semicircle, the lower impedance on electrode/electrolyte. From the magnified plot

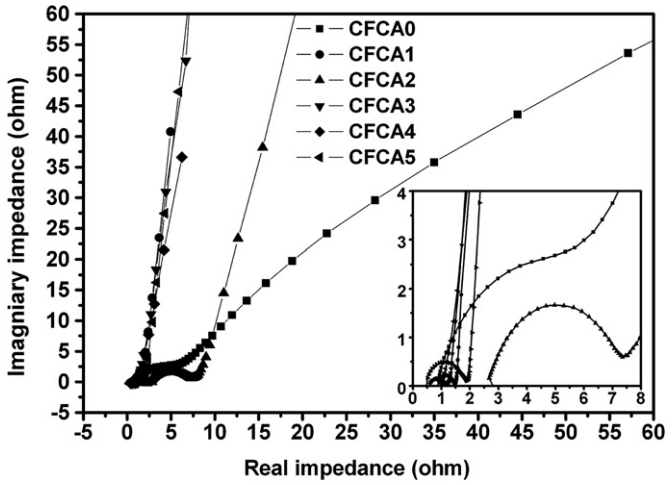

Fig. 6. Nyquist plot, showing the imaginary part against the real part of impedance, (inset) the magnified Nyquist plot for various activated CFC in 1 M H_2SO_4 at voltage amplitude of 5 mV.

(Fig. 6 inset), it can be seen that the semicircle of CFCA4 electrode material is the smallest among the six samples. Therefore, the CFCA4 electrode has better conductive property and consequent electrode chemical properties. Apparently, the plot suggests that conductive property of raw chicken feather carbon material has been improved upon the activation. The resistance variation may be related to carbon wettability, the electrical connection area of the sample, and the formation of water aggregates [30]. In the low frequency region, a straight line in the imaginary plot is observed for all activation samples, indicating the excellent capacitive behavior of the activated materials. In particular, CFCA4 electrode material possesses the superior specific capacitance that calculated from the imaginary data of the complex impedance [31]. These results show the suitability of CFCA4 as the electrode material for EDLCs.

The galvanostatic charge/discharge curves of CFCA4 at three current densities in 1 M H_2SO_4 are depicted in Fig. 7. The specific capacitance is calculated from the discharge curves according to equation:

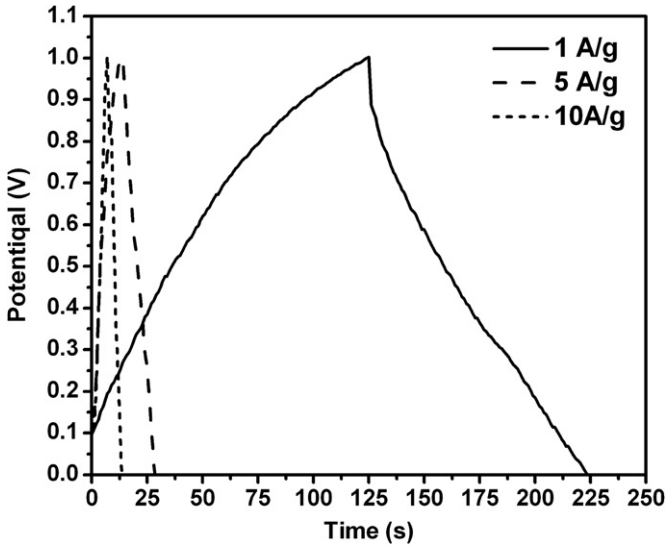

Fig. 7. Galvanostatic charge/discharge curves of the symmetric supercapacitor with CFCA4-based electrodes measured in 1 M H_2SO_4 at various current densities.

$$C = 2i\Delta t/M\Delta V \quad (2)$$

where i is the constant discharge current density, Δt the discharging time, and ΔV the potential change apart from the ohmic drop. According to Eq. (2), the specific capacitance is 278, 181, 167 F g^{-1}, respectively. It is worth noting that, although a significant reduction of the specific capacitance with the increase in current density, the specific capacitance achieved at the current density of 10 A g^{-1} is still significantly high. Moreover, the charge/discharge curves are nearly linear and almost symmetrical at three current densities, showing the excellent reversibility and capacitive property for electrode material of EDLCs. Subsequently, the voltage drop at the initiation of the discharge is 0.09 V (for the current density of 1 A g^{-1}), and enhances slightly with the increasing of current density from 1 to 10 A g^{-1}, illustrating that the excellent conductivity performance for the activated carbon materials and the lower electrochemical polarization in acid aqueous media. The voltage drop, as the results of many researchers, is attributed to the resistance of electrolytes and inner resistance of ion migration in carbon micropores [29]. These results prove that CFCA4 have developed the optimum pore size and moderate specific area. In this case, micropores act as reservoirs for electrolyte ions and facilitate ion transport through the carbon pore network at high speed of charge/discharge [31].

The average energy density and power density of CFCA4 at three current densities were estimated on the basis of the symmetric supercapacitor measurement in the 1 M H_2SO_4 for the charge to 1 V. The energy density and power density are calculated according to Eqs. (3) and (4):

$$E = 0.5CV^2 \quad (3)$$

$$P = V^2/4\mathrm{ESR}{*}M \quad (4)$$

where V is the potential region of discharge; Calculated from formula (3) and (4), the energy densities are respectively 7.98, 5.19, 4.77 Wh kg^{-1} and the power densities are respectively 1.40, 5.68, 8.35 kW kg^{-1}. In the case of the activated carbon material presented here, it can be observed that the supercapcacitor can export power density of 10 kW kg^{-1} at current density of 10 A g^{-1}.

To further investigate the electrochemical stability of capacitor with different activated carbon materials, in galvanostatic charge/discharge cycling, symmetric capacitor is repeatedly charged up to 1 V. As shown in Fig. 8, the specific capacitance of five activated CFC is decreased slowly at the current density of 1 A g^{-1}, even though after 5000 cycles. This demonstrates that the repeated charge/discharge behavior does not seem to induce the significant structure transform for all activated samples. All activated samples possess relatively stable capacitive performance with the increase in cycle number. The particular stability can be explained by the optimized high density micropores structure of the activated carbon, which allows H^+ and SO_4^{2-} to access to the surface with cycling and provides certain amount of adsorbent sites with reversible adsorption electrolyte easily. Simultaneously, the most interesting and extraordinary fact is that CFCA4 shows the superior specific capacitance of 302 F g^{-1} in comparison with others electrode material and tends to stabilize at 253 F g^{-1} after 5000 cycles. The observed higher capacitance may be attributed to the following reasons: a) the CFCA4 sample shows comparatively large pore size and wide pore distribution, which can improve the rate of ions adsorption, thus enhancing the storage capacity; b) the minority of oxygen-containing groups providing a pseudocapacitive contribution; c) the low resistance of CFCA4 has also got significant part in the capacitance improvement.

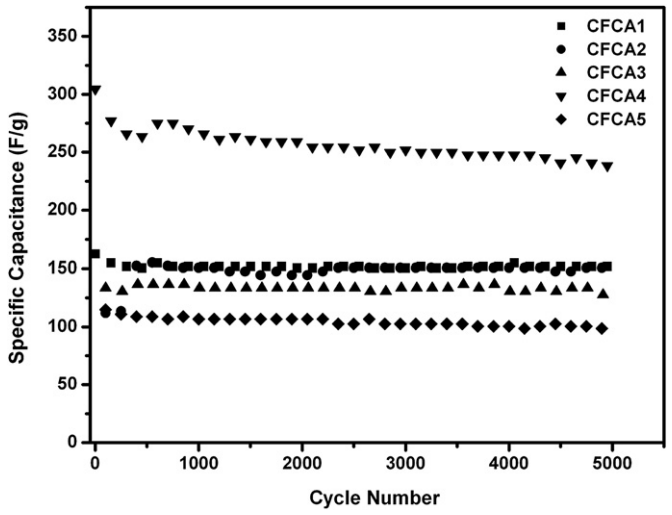

Fig. 8. The evaluation of galvanostatic charge/discharge cycling stability of the different activated at the current load of 1 A g^{-1} and cell voltage of 1 V.

4. Conclusions

In conclusion, the electrode material with excellent performance for EDLCs has been achieved by carbonization of chicken feather keratin biopolymer and activation with KOH. Activation through different weight ratios of KOH/CFC can dramatically affect electrochemical capacitance of activated carbon deriving from chicken feather keratin biopolymer in H_2SO_4 solution. The specific area and the pore structures are affected significantly by activation ratio. The morphology and amorphous nature of CFCA0 and CFCA4 have been confirmed via HR-TEM, XRD and XPS. Compared with other samples, the largest specific capacitance of 302 F g^{-1} at 1 A g^{-1} as well as the highest energy density on the gravimetric basis of 7.98 Wh kg^{-1} for CFCA4 have been achieved in 1 M H_2SO_4. Moreover, a low capacitance fading is observed after 5000 cycles, which is related to the amount of adsorbent sites with reversible adsorption electrolyte easily. Hence it could be summarized that the optimum activation ratio of KOH/CFC for the prepared activated carbon is determined to be 4. Considering that several billion pounds of chicken feather are accumulated per year and that the carbon-related material can be produced at cheap cost under more environmentally friendly conditions, the preparation route is prospective for supercapacitors electrode material industry.

Acknowledgments

The authors gratefully appreciate the supports from the Youth Project of National Nature Science Foundation of China (Grant No. 51103124 and 51203131) and Hunan province universities innovation platform of Open Fund Project (11K067).

References

[1] B.E. Conway, Electrochemical Supercapacitors: Scientific Fundamentals and Technological Applications, Kluwer Academic/Plenum Publishers, New York, 1999.
[2] A. Burke, J. Power Sources 91 (2000) 37–50.
[3] X.J. He, Y.J. Geng, J.S. Qiu, M.D. Zheng, S. Long, X.Y. Zhang, Carbon 48 (2010) 1662–1669.
[4] G. Lota, J. Tyczkowski, R. Kapica, K. Lota, E. Frackowiak, J. Power Sources 195 (2010) 7535–7539.
[5] J.W. Lang, X.B. Yan, X.Y. Yuan, J. Yang, Q.J. Xue, J. Power Sources 196 (2011) 10472–10478.
[6] C.C. Hu, K.H. Chang, M.C. Lin, Y.T. Wu, Nano. Lett. 6 (2006) 2690–2695.
[7] M. Toupin, T. Brousse, D. Belanger, Chem. Mater. 16 (2004) 3184–3190.
[8] E. Raymundo-Piñero, F. Leroux, F. Béguin, Adv. Mater. 18 (2006) 1877–1882.
[9] W. Xiong, M.X. Liu, L.H. Gan, Y.k Lv, Y. Li, L. Yang, Z.J. Xua, Z.X. Hao, H.L. Liu, L.W. Chen, J. Power Sources 209 (2012) 152–155.
[10] L. Zhao, L.Z. Fan, M.Q. Zhou, H. Guan, S.Y. Qiao, M. Antonietti, M.M. Titirici, Adv. Mater. 22 (2010) 5202–5206.
[11] Y.P. Zhai, Y.Q. Dou, D.Y. Zhao, P.F. Fulvio, R.T. Mayes, S. Dai, Adv. Mater. 23 (2012) 4828–4850.
[12] E. Frackowiak, F. Beguin, Carbon 39 (2001) 937–950.
[13] T.C. Weng, H. Teng, J. Electrochem. Soc. 148 (2001) 368–373.
[14] F.C. Wu, R.L. Tseng, C.C. Hu, C.C. Wang, J. Power Sources 159 (2006) 1532–1542.
[15] Z. Li, L. Zhang, B.S. Amirkhiz, X.H. Tan, Z.W. Xu, H.L. Wang, B.C. Olsen, C.M.B. Holt, D. Mitlin, Adv. Energy Mater. 2 (2012) 431–437.
[16] E. Senoz, R.P. Wool, J. Appl. Polym. Sci. 118 (2010) 1752–1765.
[17] L. Dossey, Explore J. Sci. Healing 1 (2005) 155–158.
[18] G. Salitra, A. Soffer, L. Eliad, Y. Cohen, D. Aurbach, J. Electrochem. Soc. 147 (2000) 2486–2493.
[19] Z.H. Hu, M.P. Srinivasan, Y.M. Ni, Adv. Mater. 12 (2000) 62–65.
[20] V. Subramanian, C. Luo, A.M. Stephan, K.S. Nahm, S. Thomas, B.Q. Wei, J. Phys. Chem. C 111 (2007) 7527–7531.
[21] M.A. Lillo-Ródenas, D. Cazorla-Amorós, A. Linares-Solano, Carbon 41 (2003) 267–275.
[22] R. Tseng, S. Tseng, J. Colloid Interface Sci. 287 (2005) 428–437.
[23] Y.P. Guo, S.F. Yang, K. Yu, J.Z. Zhao, Z.C. Wang, H.D. Xu, Mater. Chem. Phys. 74 (2002) 320–323.
[24] J.A. Leiro, M.H. Heinonen, T. Laiho, I.G. Batirev, J. Electron. Spectrosc. Relat. Phenom. 128 (2003) 205–213.
[25] H. Teng, Y.J. Chang, C.T. Hsieh, Carbon 39 (2001) 1981–1987.
[26] L.G. Austin, E.G. Gagnon, J. Electrochem. Soc. 120 (1973) 251–254.
[27] S. Biniak, A. Swiatkowski, M. Makula, in: L.R. Radovic (Ed.), Chemistry and Physics of Carbon, Marcel Dekker, New York, 2001 (chapter 3).
[28] B. Dong, B. He, C. Xu, H. Li, Mater. Sci. Eng. B 143 (2007) 7–13.
[29] W. Lu, G. Yushin, Carbon 49 (2011) 4830–4838.
[30] Y.R. Nian, H. Teng, J. Electrochem. Soc. 149 (2002) 1008–1014.
[31] X. Liu, T. Osaka, J. Electrochem. Soc. 144 (1997) 3066–3071.